



## Light absorption and fluorescence properties of chromophoric dissolved organic matter (CDOM), in the St. Lawrence Estuary (Case 2 waters)

B. NIEKE,\* R. REUTER,† R. HEUERMANN,† H. WANG,‡  
M. BABIN§ and J. C. THERRIAU¶

(Received 11 January 1996; accepted 30 April 1996)

**Abstract**—The absorption coefficient and the fluorescence emission of chromophoric (coloured) dissolved organic matter (CDOM) were determined along a 1200 km transect in the Estuary and Gulf of St. Lawrence. Fluorescence spectra were spectrally corrected against a reference standard and normalized to the water Raman signal to provide results in Raman units. Because CDOM originates mainly from freshwater river runoff in the St. Lawrence system, its optical properties were found to be inversely correlated with salinity ( $r = -0.95$ ) and sigma- $t$  ( $r = -0.99$ ). These strong linear relationships can be used as a tool for monitoring surface circulation and salinity in these coastal waters. The relationships between CDOM absorption and fluorescence were also characterized in the UV and visible regions. In the UV region, the observed relationship was found to be consistent with previously published results. In the visible region a relationship was found that was different from that in the UV. Our results therefore support the possibility of using fluorescence characteristics for extensive monitoring of CDOM in coastal waters strongly influenced by freshwater runoff. Such relationships may prove useful for remote sensing to correct chl  $a$  values and the large-scale modelling of primary production in coastal waters. Copyright © 1996 Elsevier Science Ltd

### 1. INTRODUCTION

Morel and Prieur (1977) partitioned marine waters in two general categories on the basis of their bulk optical properties: oceanic (Case 1) waters and coastal (Case 2) waters. Following the nomenclature (Gordon and Morel, 1983; Morel, 1988), “Case 1” includes those waters where variations in optical properties are mainly governed by the abundance of phytoplankton. “Case 2” waters are those where optical properties are influenced by phytoplankton and, additionally, by organic and inorganic particulate and dissolved organic matter of local and terrestrial origin (non-chlorophyllous matter).

In Case 1 waters, the relative proportions of phytoplankton and related derivatives are

---

\*Département de Biologie, Université Laval, Sainte Foy, Québec G1K 7P4, Canada.

†Carl von Ossietzky Universität Oldenburg, Fachbereich Physik, D-26111 Oldenburg, Germany.

‡Physikalisch Technische Bundesanstalt, D-38100 Braunschweig, Germany.

§LPCM, Université Pierre et Marie Curie, F-06230 Villefranche sur mer, France.

¶Institut Maurice-Lamontagne, Ministère des Pêches et des Océans, CP 1000, Mont-Joli, Québec G5H 3Z4, Canada.

well correlated with chl *a* concentration ( $\langle \text{chl} \rangle$ ) (Morel and Prieur, 1977; Baker and Smith, 1982; Carder *et al.*, 1986) and, consequently, the vertical propagation of light can be estimated using simple models relating  $\langle \text{chl} \rangle$  to the vertical diffuse attenuation coefficient,  $K_d$  (Baker and Smith, 1982; Morel, 1988). However, it is not possible to use such an approach for Case 2 waters. The simple optical behaviour of Case 1 waters has led to successful applications of ocean colour remote sensing, in deriving large-scale maps of  $\langle \text{chl} \rangle$  (André and Morel, 1991). Chlorophyll *a* concentration and light absorption are the key input variables in primary production models (e.g. Platt and Sathyendranath, 1988), and these variables can thus be used to derive maps of primary production (e.g. André and Morel, 1991). For Case 2 waters, humic and fulvic acids (often called yellow substance or gelbstoff, following Kalle, 1938), which represent about 70% of the dissolved organic matter (DOM) (Spitzzy and Ittekkot, 1986), significantly contribute to light absorption and fluorescence by non-chlorophyllous material. These substances are referred to here as chromophoric or coloured DOM (CDOM). These substances strongly influence the underwater light field and, hence, the penetration of photosynthetically active radiation, due to their significant absorption at UV and blue wavelengths (Kalle, 1938; Diehl and Haardt, 1980; Bricaud *et al.*, 1981; Reuter *et al.*, 1986). CDOM is thus a key parameter in bio-optical models of primary production for Case 2 waters.

In coastal waters and neighbouring areas, absorption by non-chlorophyllous substances often largely exceeds that by phytoplankton (Carder *et al.*, 1991). CDOM originates from the degradation of phytoplankton and, especially in coastal waters, from land drainage. It is therefore widely used as an optical tracer to investigate the transport and mixing processes in estuarine and coastal zones. It is measured using *in situ* or laboratory methods (Duursma, 1974; Dorsch and Bidleman, 1982; Willey and Atkinson, 1982; Willey, 1984; Hayase *et al.*, 1987; Chen and Bada, 1992), or airborne remote sensing techniques (e.g. Hope and Swift, 1982; Barlow *et al.*, 1985; Reuter *et al.*, 1993). One problem, however, is that the relative proportions between phytoplankton and the other absorbing substances do not follow any specific trend. As a consequence, in Case 2 waters, the vertical propagation of light cannot be easily predicted for use in large-scale primary production models. Moreover, since CDOM strongly absorbs in the spectral region where chl *a* exhibits maximum absorption, its presence leads to a strong bias in remote sensing estimates of  $\langle \text{chl} \rangle$ , such as those derived from the Coastal Zone Colour Scanner (CZCS).

To overcome this problem, most of the space agencies (NASA, NASDA, ESA) have planned to add a band at *ca* 410–420 nm in their future ocean colour sensors. Since absorption by phytoplankton pigments is lower in this spectral range, these measurements are expected to provide an estimation of absorption by non-chlorophyllous matter. A reflectance model has been proposed by Carder *et al.* (1991) in order to incorporate such information in remote sensing data processing. This will call for extensive monitoring at sea of absorption properties, since this model is expected to be site- and season-specific.

Besides absorption properties of CDOM, fluorescence emission is another optical characteristic widely used for investigating CDOM distributions in Case 2 waters (e.g. Kalle, 1963; Traganza, 1969; Duursma, 1974). Direct measurements of CDOM absorption in seawater are generally time consuming and often limited by the sensitivity of conventional spectrophotometers. For this reason, Hoge *et al.* (1993) recently proposed a technique relying on the close relationship that exists between the absorption and fluorescence of CDOM in the UV range. This technique provides a fast and sensitive tool for estimating CDOM and can be easily extended to airborne active remote sensing

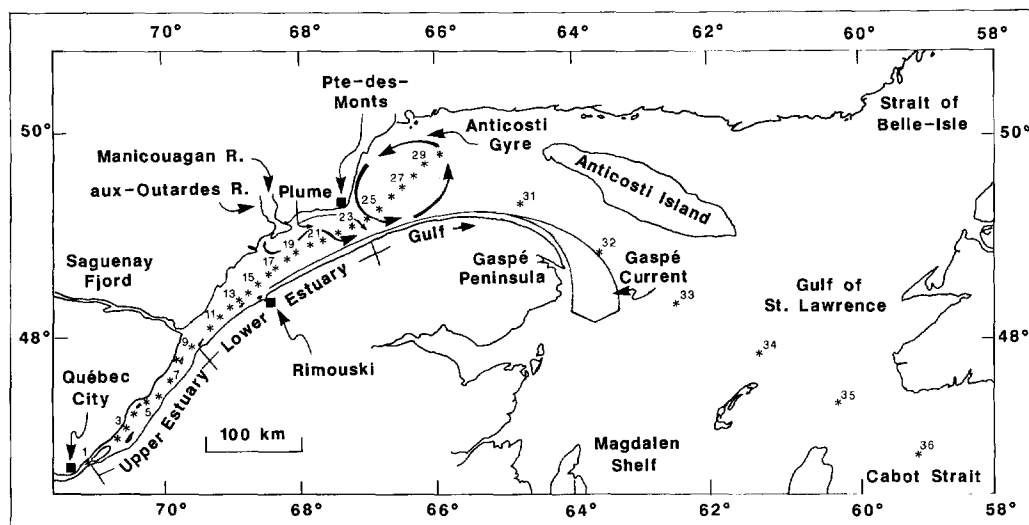


Fig. 1. Location of the sampling stations along the 1200 km transect in the Estuary and Gulf of St. Lawrence and circulation patterns derived from the literature and remote sensing maps (El-Sabh, 1979).

techniques (e.g. lidar). This approach may thus be the best way for interpreting remotely sensed ocean colour data in Case 2 waters.

The first objective of the present study was to characterize the relationship between fluorescence or absorption of CDOM in the visible range and salinity in the St. Lawrence system and to determine if these optical characteristics could be used to study surface circulation there. The second objective was to derive a relationship between fluorescence and visible light absorption of CDOM, since data collected in the visible region of the light absorption spectrum might be more pertinent in the context of primary production studies and to compare this relationship to those of Hoge *et al.* (1993) in the UV region.

## 2. MATERIALS AND METHODS

### 2.1. The St. Lawrence system

The Estuary and Gulf of St. Lawrence system (Canada) is an excellent natural laboratory to validate remote sensing data, since it provides, over a relatively small horizontal scale, a wide gradient of hydrographic conditions, from Case 2 to Case 1 waters, with superimposed local structures such as runoff plumes, upwelling areas, gyres, fronts, etc.

The St. Lawrence system is a highly stratified, semi-enclosed water body, with connections to the Atlantic Ocean through Cabot and Belle-Isle Straits (Fig. 1). It can be divided into three main regions: the Upper Estuary, the Lower Estuary, and the Gulf itself (Brunel, 1970; El-Sabh *et al.*, 1979). The Upper Estuary, with depths averaging 60 m, is characterized by a strong surface salinity gradient from fresh waters near Québec City to waters of salinity *ca* 20 psu near the mouth of the Saguenay Fjord, where bottom topography drops abruptly to >200 m over a few kilometres. The Lower Estuary, which extends from the Saguenay Fjord to Pointe-des-Monts, is characterized by surface

salinities varying between 20 and 30 psu. The spatial distribution of these surface waters shows a strong influence of physical features such as an upwelling zone near the mouth of the Saguenay Fjord (Forrester, 1974; Therriault and Lacroix, 1976), a large fresh-water plume originating from the Manicouagan and Aux-Outardes rivers (Therriault and Levasseur, 1985, 1986; Therriault *et al.*, 1985), and the Gaspé coastal jet current flowing along the Gaspé peninsula (Tang, 1980; El-Sabh, 1979) which results from the combination of surface outflows from the Estuary, the Saguenay Fjord and the Manicouagan/Aux-Outardes plumes. The surface waters of the Gulf are mostly characterized by oceanic type waters, which reflect their connection with the Atlantic Ocean through the Cabot and Belle-Isle straits (Fig. 1). Two major hydrographic features in the southwestern part of the Gulf are the Anticosti Gyre and the Gaspé Current (Fig. 1; El-Sabh, 1976). The southwestern region of the Gulf is strongly influenced by the Gaspé Current outflow.

Surface circulation in the St. Lawrence system is mainly governed by freshwater input from the Upper Estuary and other affluent rivers and by seawater entering the Gulf through Belle-Isles and Cabot Straits (Neu, 1970). Freshwater runoff reaches highest values between June and August. Combination of the latter factor with seasonal heating of the surface layer and tidal currents produces a typical summer circulation pattern and distribution of water masses, which are described in detail in the review of Koutitonski and Bugden (1991) and whose main characteristics have been mentioned above. Because of the size of the system, a synoptic overview cannot be obtained by shipboard measurements.

## 2.2. *Sampling and chl a*

Sampling was conducted at 36 stations located along a 1200 km transect in the Estuary and the Gulf of St. Lawrence (Fig. 1), from 3 to 20 July 1990. Water samples were collected at a depth of  $2.4 \pm 0.2$  m, using a rosette sampler equipped with five GoFlo bottles. Temperatures and salinity profiles were recorded down to the depth of 1% surface irradiance, using a CTD probe (APPLIED MICROSYSTEMS, model STD-12) attached to the rosette. The vertical profile of photosynthetically available radiation (PAR = 400–700 nm) was determined using a quantameter equipped with a  $4\pi$  underwater collector and a deck reference sensor (BIOSPHERICAL, model QSP-240). Immediately after collection, water samples were poured into 4 l clean amber glass bottles. These bottles were stored at 15°C and measurements done within the following 2 h. Before dividing the sample into subsamples for individual analyses, the bottles were gently shaken to resuspend particles. Subsamples were filtered onto GF/F Whatman filters for the determination of chl *a* and phaeopigment concentrations using the fluorometric method of Yentsch and Menzel (1963) as modified by Holm-Hansen *et al.* (1965), after extraction in 90% acetone.

## 2.3. *Spectral CDOM fluorescence*

The emission spectrum of CDOM was measured using a laboratory spectrofluorometer (PERKIN ELMER LS50). Table 1 gives the excitation wavelengths, the range of emission wavelengths and the instrument setup used for measurements. The excitation lines were selected to be close to the emission wavelengths of light sources which are often used in fluorescence spectroscopy, such as the 365 nm mercury line, the 382 nm laser dye

Table 1. Fluorescence spectra characterization of the PERKIN ELMER LS50 instrument

	Excitation (ex)		
	365 nm	388 nm	480 nm
Emission (em)	380–550 nm	410–550 nm	510–700 nm
Slits (em/ex)	10 nm/10 nm		
Scan speed	240 nm min <sup>-1</sup>		
Resolution	0.5 nm		
em filter		Schott WG320	Schott WG320
Raman	416.7 nm	447 nm	573.6 nm
FDOM peak	460 nm	490 nm	
Chl <i>a</i> peak			685 nm

maximum (LAMBDA PHYSICS, FL-150), and the 488 nm emission of argon ion lasers. Before use, the quartz cuvettes were pre-cleaned with MUCASOL (MERCK), rinsed several times in purified water (MILLIPORE), soaked in 20% HNO<sub>3</sub>, rinsed with pure water, and soaked again in MUCASOL. After a final rinse with purified water, the cuvettes were pre-dried at ambient temperature under dust protection and finally dried during 4 h at 200°C. The cuvettes were rinsed three times with the sample using pre-cleaned Pasteur pipettes, prior to immediate measurements. A four position automatic sample holder was used to speed up measurement procedures.

The stability of the xenon flash lamp used as light source and the spectral correction of the excitation monochromator were achieved using a built in instrument setup. Calibration of the emission monochromator and red-sensitive photomultiplier tube, which was used for signal detection, was done on a daily basis as recommended by Childs (1989) with a solution (1 ppm) of quinine sulphate dihydrate ( $1.28 \times 10^{-6}$  mol l<sup>-1</sup>) in HClO<sub>4</sub> (0.105 mol l<sup>-1</sup>), prepared following the NBS procedure (Velapoldi and Mielenz, 1980).

The conversion of fluorescence readings into quantitative spectral information was done by using the water Raman scatter band to calibrate the individual wavelength readings. The Raman signal is a well-defined signal with known quantum efficiency and line shape, which is present in all measured spectra. It shows a well-defined dependence on the excitation wavelength. Calibration was done by dividing the fluorescence intensity at a given emission wavelength by the water Raman scatter band integrated over its entire bandwidth. Since signal intensities taken at specific wavelengths are normalized to intensities integrated over a wavelength interval, data are thus in units of inverse wavelength (nm<sup>-1</sup>), which are denoted as "Raman units". The advantage of normalizing by the integral water Raman scatter band, and hence of using Raman units to measure the concentration of fluorescent substances, is that normalized data can be quantitatively reproduced with any type of fluorometer, which includes *in situ* probes and airborne fluorosensors. The only requirement is to use a spectrometer which is spectrally calibrated and capable of detecting the water Raman scatter band accurately. Detailed discussion of this calibration procedure can be found in Determann *et al.* (1994).

In order to numerically compare the fluorescence data obtained with different excitation wavelengths, the inverse fourth power dependence of the Raman band intensity on the excitation wavelengths must be taken into account. For example, the water Raman

signal excited with 275 nm wavelength is approximately 10 times stronger than that excited at 488 nm, which correspondingly affects the value of Raman normalized fluorescence data. The absolute accuracy of fluorescence readings depends on several factors such as the chosen excitation and emission wavelengths, the concentration of fluorescent material, and sample treatment. The accuracy of results in the present paper is estimated to be in the range of 0.001–0.01 nm<sup>-1</sup> Raman units. The reproducibility of fluorescence readings was typically better than  $\pm 10\%$

#### 2.4. Spectral absorption coefficients of CDOM and attenuation coefficients of particulate matter

The absorption coefficients of water samples were measured over the 350–700 nm range, with 10 nm increments, using a custom built spectrophotometer equipped with a 1 m optical pathlength cuvette. This instrument was introduced by Haardt *et al.* (1979). The cuvette, which has a sample volume of 2.5 l, is made of stainless steel coated with TEFLON. A 150 W OSRAM XENOPHOT HXL halogen lamp is used as the light source. Monochromatic light is obtained with a grating monochromator (INSTRUMENT SA H-20) with an optical bandwidth of 5 nm. Its output aperture is used to produce a nearly parallel light beam, which enters and exits the sample cuvette through quartz windows. Scattered light is discriminated by a telescope setup which has a 0.3° field of view. The signal is detected by a photomultiplier (HAMAMATSU 1P28) placed at the telescope focal plane. To prevent settling of particulate matter during the measurement, the sample volume is continuously circulated in the cuvette using a peristaltic pump.

Spectral values of the absorption coefficient of CDOM ( $a_{\text{CDOM}}$ ) were measured on seawater samples filtered on to SARTORIUS cellulose nitrate filters (0.2  $\mu\text{m}$  pore size), with purified water as reference medium (MILLIPORE). In order to obtain the spectral attenuation coefficients of particulate matter ( $cp$ ), measurements were made on unfiltered samples against MILLIPORE water. Computing the difference between total attenuation and  $a_{\text{CDOM}}$  gave  $cp$ . Because absorption measurements were time consuming, these could not be done at all stations. In addition, the concentration of particulate matter in the Upper Estuary was often too high to allow measurement of unfiltered samples from many stations with our instrument. This results in sampling gaps in the upper and lower estuarine regions where, however, distances between stations were small.

In addition to instrumental factors such as stability of the lamp intensity and detector sensitivity, the accuracy of absorption coefficients depends on the quality of purified water used as the reference medium. The importance of the latter is a function of the concentration of suspended and dissolved material, which is also true for the accuracy of the calculated attenuation coefficient (Austin and Petzold, 1977; Austin, 1977). Moreover, because of the long beam path, it is difficult to maintain an accurate optical alignment, which leads to additional uncertainty. We estimated the relative error of  $a_{\text{CDOM}}$  to be *ca* 10% in the range of  $a_{\text{CDOM}} < 3 \text{ m}^{-1}$  and *ca* 50% in the range of  $a_{\text{CDOM}} < 1 \text{ m}^{-1}$ .

### 3. RESULTS

#### 3.1. Spatial distribution of oceanographic variables

Figure 2 illustrates the spatial variations at 2 m depth of (a) surface temperature and salinity, (b) the sum of chl *a* and phaeopigment concentrations, (c) the depth of 1% surface irradiance, as an indicator of the extent of the euphotic zone, (d) the absorption

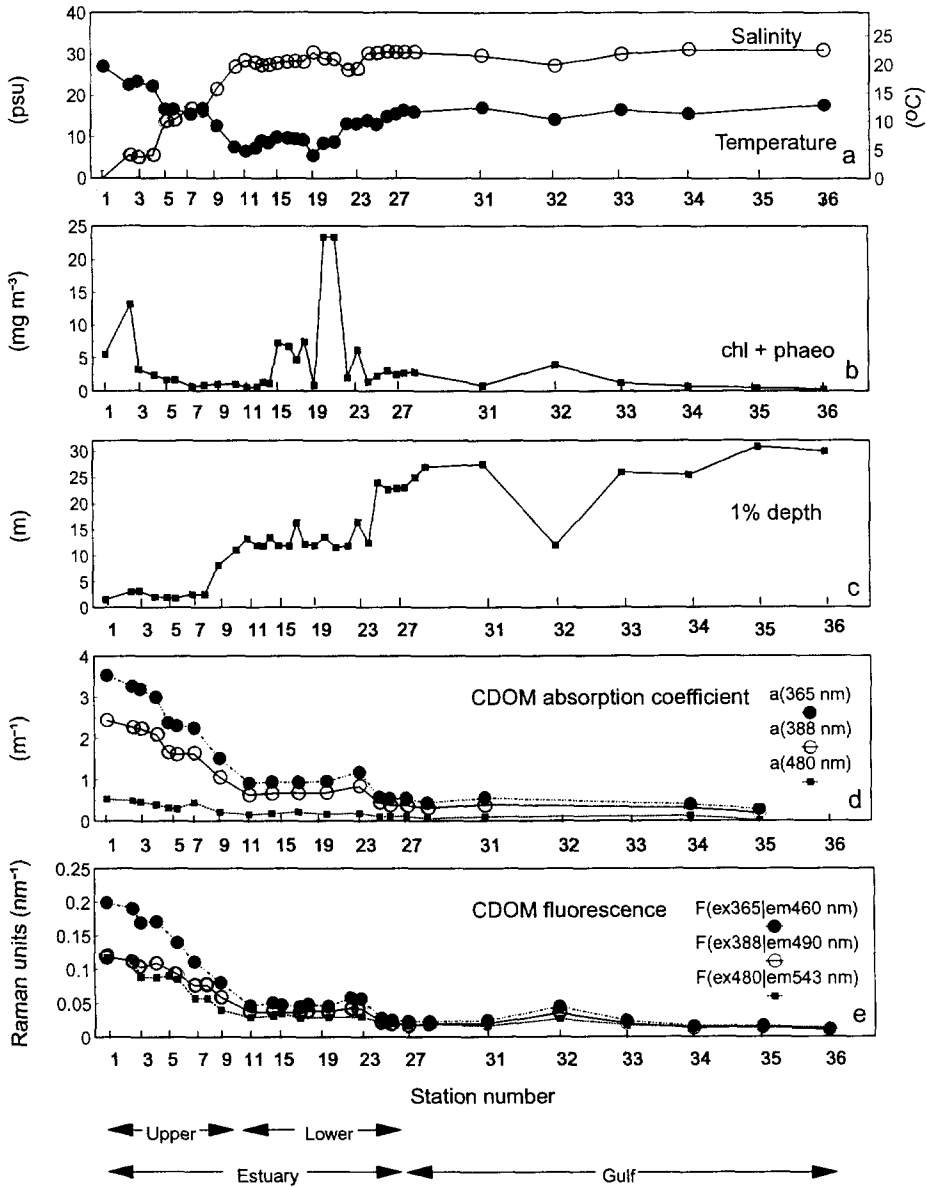


Fig. 2. Distributions of (a) surface temperature and salinity, (b) the sum of chl *a* and phaeo-pigments, (c) the depth of 1% surface PAR, (d) CDOM absorption coefficients, and (e) CDOM fluorescence at 2 m depth along the 1200 km transect in the St. Lawrence system.

coefficients of CDOM at 365, 388 and 480 nm, and (e) the fluorescence of coefficients of CDOM at 365, 388 and 480 nm, and (e) the fluorescence of CDOM excited at 365, 388 and 480 nm and emitted at 460, 490 and 543 nm, respectively, along the transect from Québec City to Cabot Strait (Fig. 1). Since sigma-*t* and salinity were strongly correlated in the surface waters of the St. Lawrence system, salinity only is used in this paper.

Mixing between freshwater from river runoff and saltwater mainly occurred in the Upper Estuary, downstream from Québec City (Sta. 1) to the Saguenay Fjord (Stas 9–10). Salinity increased almost linearly with distance over this part of the transect, from 0 to 20 psu, and temperature decreased from 22 to 14°C. This region of the Estuary was characterized by the most turbid waters, the depth of the euphotic zone never exceeding 3 m in the Upper Estuary [Fig. 2(c)]. Chl *a* + phaeopigments (chl + phaeo) concentrations in the area showed higher values at the first two stations (typically freshwater) and very low values up to the mouth of the Saguenay Fjord [Fig. 2(b)]. This corresponds to the region where intense mixing of fresh and salt water occurs. Figures 2(d) and 2(e) also show that highest values of absorption and fluorescence were observed at all wavelengths in the freshwater region. A regularly decreasing gradient of fluorescence and absorption paralleled the increasing salinity gradient, up to Sta. 9.

Stations 10–24 correspond to the Lower Estuary and were characterized by euphotic depths between 11 and 15 m. Surface waters were characterized by salinities from *ca* 25 to 28 psu and temperatures from *ca* 5 to 10°C. Concentrations of chl + phaeo were variable and higher than in the Upper Estuary [Fig. 2(b)]. Further down in the Lower Estuary, salinity, temperature, and euphotic zone depth remained quite constant (*ca* 27 psu, 8°C and 15 m, respectively). Chl + phaeo concentrations were, however, quite variable with bloom levels at Stas 20 and 21 which correspond to the region where the plume of the combined Manicouagan and Aux-Outardes rivers is most apparent (Therriault and Levasseur, 1986). Values of absorption and fluorescence [Fig. 2(d) and (e)] were intermediate between those observed upstream and downstream with an increase in the plume area. Attenuation coefficients of particulate matter closely followed the trend of  $a_{\text{CDOM}}$  and  $F_{\text{CDOM}}$  and were in the range of 3–2 m<sup>-1</sup> (not shown).

Stations 24–30 were located in the Anticosti Gyre, which is a major feature in the northwestern region of the Gulf and whose water mass characteristics are typical of Case 1 waters (Babin *et al.*, 1993). Salinity and temperature were relatively high (>30 psu and 15°C) and the euphotic depth reached *ca* 25 m. Chl + phaeo concentrations were moderately lower than upstream (2.5 mg m<sup>-3</sup>) reflecting the nutrient depleted summer conditions (Therriault and Levasseur, 1985). Absorption and fluorescence values were low and *cp* decreased to values between 1 and 0.5 m<sup>-1</sup> (not shown).

Stations 31–36 are located along the transect from the Anticosti Gyre to Cabot Strait. Relatively lower temperature and salinity, higher biomass, and shallower euphotic zone at Sta. 32 corresponded to the Gaspé Current (Fig. 2). This jet current flows near the south shore of the Estuary and reaches its highest intensity along the Gaspé Peninsula, before spreading on the Magdalen Shelf (Benoît *et al.*, 1985). These same variables (Fig. 2) indicated that Stas 31–36 were located outside the Gaspé Current. In their surface waters, biomass was low (1 mg m<sup>-3</sup>), the euphotic zone was deep (up to 30 m except for Sta. 32), absorption and fluorescence values were low, and *cp* values were *ca* 0.5 m<sup>-1</sup> (not shown).

### 3.2. Relationship between dissolved organic matter fluorescence and absorption with salinity

Figure 3 shows examples of fluorescence spectra from surface water at one station, with three different excitation wavelengths. This figure illustrates the typical fluorescence signatures observed along the whole transect. All three spectra clearly show the Raman

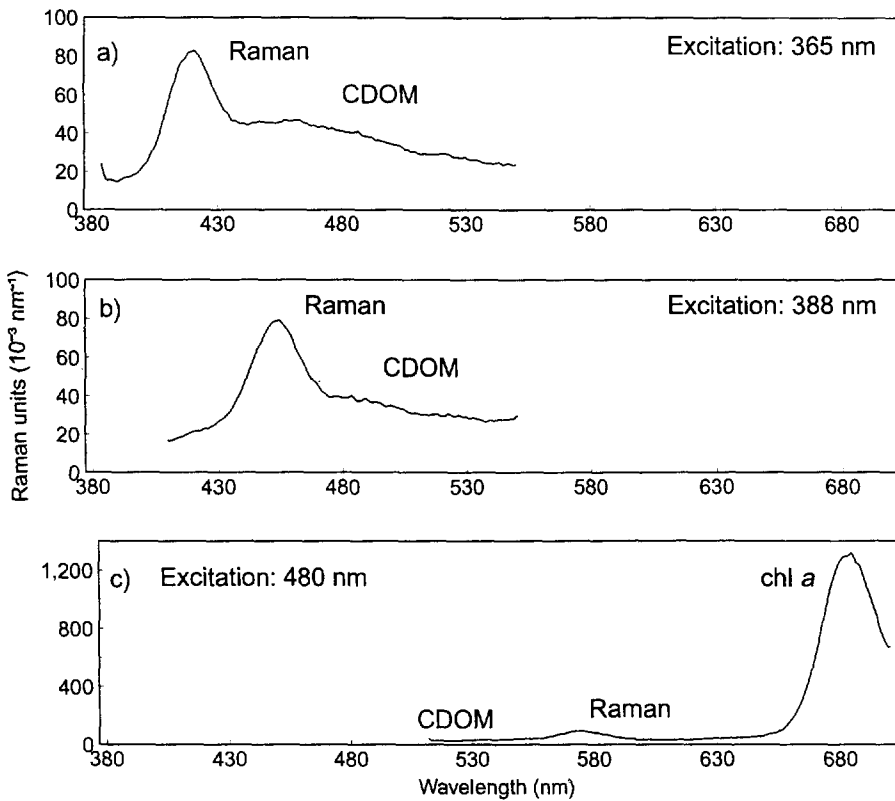


Fig. 3. Seawater fluorescence emission spectra with three different excitation wavelengths, displaying (a,b) Raman and  $F_{\text{CDOM}}$  and (c) Raman,  $F_{\text{CDOM}}$  and chl *a* fluorescence of surface water at Sta. 20.

signal. Figure 3(a) and (b) shows high emission of  $F_{\text{CDOM}}$  at 460 and 490 nm, respectively, for the 365 and 388 nm excitation wavelengths. Figure 3(c) (480 nm excitation) did not exhibit a signal corresponding to  $F_{\text{CDOM}}$ , but it showed a strong chl *a* fluorescence peak at 685 nm.

Typical  $a_{\text{CDOM}}$  spectra are given in Fig. 4. The spectra with highest absorption values were obtained near Québec City. From there, absorption decreased steadily along the transect toward Cabot Strait. Typically, spectral absorption  $a$  ( $\text{m}^{-1}$ ) by CDOM between  $\lambda = 350$  and 700 nm obeys a relationship of the form (Bricaud *et al.*, 1981):

$$a_{\text{CDOM}}(\lambda) = a_{\text{CDOM}}(\lambda_0) \exp\{-S(\lambda - \lambda_0)\}, \quad (1)$$

where  $a_{\text{CDOM}}(\lambda_0)$  is the absorption coefficient at an arbitrary wavelength within that interval and  $S$  ( $\text{nm}^{-1}$ ) determines the exponential decay of absorption with increasing wavelength. In our study, the mean value for  $S$  was  $0.015 \text{ nm}^{-1}$  ( $\pm 0.002$ ), which is in the same range as earlier reported values from various regions (Table 2).

Figure 5(a) and (c) shows the strong linear relationship between absorption or fluorescence emission (em) at different excitation (ex) wavelengths and salinity. Correlation coefficients varied from  $-0.95$  to  $-0.99$  ( $P < 0.001$ ), with the highest correlation

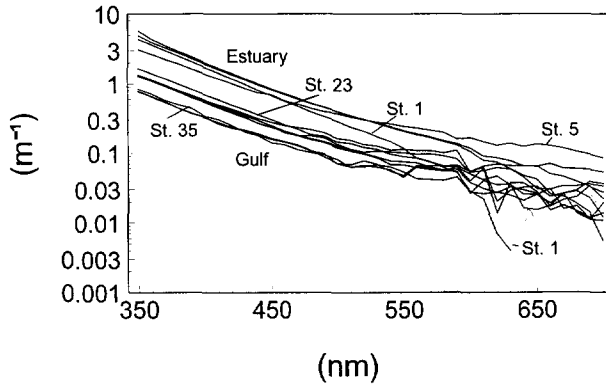


Fig. 4. Seawater absorption spectra  $a_{\text{CDOM}}$  (350–700 nm), measured with a 1 m pathlength cuvette.

Table 2. Mean values of coefficient  $S$  in the spectral dependence law for absorption:  $a_{\text{DOM}}(\lambda) = a_{\text{DOM}}(\lambda_0)\exp\{-S(\lambda - \lambda_0)\}$  ( $\lambda$  and  $\lambda_0$  in nm), in different regions of the world

$S$ ( $\text{nm}^{-1}$ )	Sampling site	Reference
0.015	St. Lawrence system	This study
0.014	Adriatic Sea	Diebel, 1987
0.011	Elbe River Estuary	Diebel, 1987
0.017	Weser River Estuary	Diebel, 1987
0.016	German Bight	Diebel, 1987
0.014	Oceanic waters	Bricaud <i>et al.</i> , 1981
0.016	Coastal zones	Bricaud <i>et al.</i> , 1981
0.013	Estuaries	Bricaud <i>et al.</i> , 1981
0.011	Elbe River Estuary	Doerffer, 1979
0.015	Baltic Sea	Lundgren, 1976
0.014	Mauritanian upwelling	Morel and Prieur, 1976
0.015	Gulf of Mexico	Maul and Gordon, 1975

coefficients being at the shortest wavelengths. Figure 5 also indicates that, for both absorption and fluorescence emission, slopes were different among wavelengths. The slopes of  $a_{\text{CDOM}}$  against salinity decreased quite regularly from 365 to 480 nm, whereas for  $F_{\text{CDOM}}$  the relationship at 365 nm was distinct from the two others which were almost identical (contrary to absorption at these two wavelengths). For  $a_{\text{CDOM}}$  and  $F_{\text{CDOM}}$  at 365 and 388 nm, a slope discontinuity occurred at salinity *ca* 29 psu. In Figure 5(b) and (d) the regression lines between salinity and optical measurements were computed on the same data sets as in Fig. 5(a) and (c), but after being split at 29 psu. Differences between the slopes of salinities >29 psu and <29 psu were tested using *t*-tests (two-tailed; Glantz, 1992). There were significant differences in slopes for 365 nm ( $P > 0.001$ ) and 388 nm ( $P > 0.01$ ), with correlation coefficients  $r = -0.99$  at salinity >29 psu and  $-0.73 > r > -0.83$  at salinity >29 psu. For 480 nm, splitting the data set did not change the regression lines.

The attenuation by particulate matter in the Lower Estuary and the Gulf at different

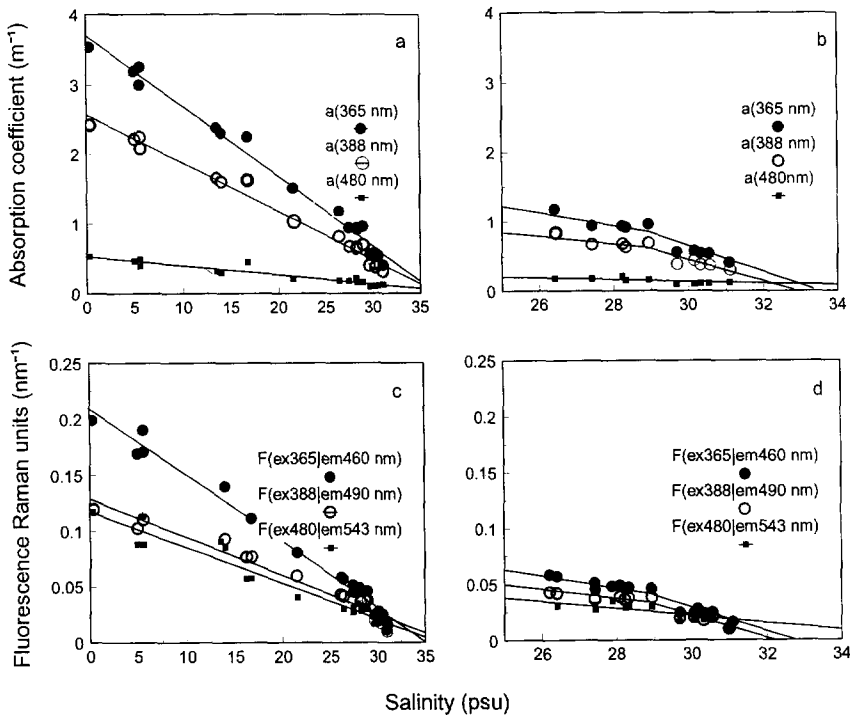


Fig. 5. Scatter diagrams and linear regressions (model 2) between salinity and (a,b)  $a_{\text{CDOM}}$  at 365, 388 and 480 nm and (c,d)  $F_{\text{CDOM}}$  emission at 460, 490 and 543 nm, excited with 365, 388 and 480 nm, respectively (all data from 2 m depth). Data are the same in the two left and two right-hand panels but, in the right-hand ones, the data sets were split at 29 psu to compute two different regressions.

wavelengths was also inversely correlated with salinity. Correlation coefficients ranged from  $-0.80$  to  $-0.83$  ( $P < 0.01$ ). Forward stepwise linear regressions of salinity against  $a_{\text{CDOM}}$ ,  $cp$  and  $\langle chl \rangle$  showed that salinity can be estimated significantly at 365, 380, and 480 nm using a linear combination of  $a_{\text{CDOM}}$  ( $P < 0.0001$ ) and  $cp$  ( $P < 0.01$ ). Including  $\langle chl \rangle$  did not significantly improve the estimation of salinity.

### 3.3. Relationship between dissolved organic matter fluorescence and absorption

High positive correlation between  $a_{\text{CDOM}}$  and  $F_{\text{CDOM}}$  were found at 365, 388, and 480 nm (Table 3 and Fig. 6). As expected, the highest correlation coefficients were observed when absorption was measured at the wavelength used to stimulate fluorescence ( $\lambda_{\text{EX}}$ ) ( $r = 0.98$ – $1.00$ ). Correlations decreased slightly with increasing wavelength (for example,  $r = 1.00$  at 365 nm and  $r = 0.98$  at 480 nm).

The following relationships between  $a_{\text{CDOM}}$  ( $\text{m}^{-1}$ ) and  $F_{\text{CDOM}}$  in Raman units ( $\text{nm}^{-1}$ ) in the UV (365 and 388 nm) and visible (480 nm) were computed. Results also give the standard error of the slope and the intercept.

$$a_{\text{CDOM}}(365) = 17.12 (\pm 0.27) F_{\text{CDOM}}(\text{ex365/em460}) + 0.12 (\pm 0.09) \quad (2)$$

Table 3. Correlation coefficients ( $r$ ) between  $a_{CDOM}$ ,  $cp$  ( $\lambda$  in nm) and  $F_{CDOM}$  ( $\lambda_{ex}/\lambda_{em}$  both in nm); 20 data pairs (Fig. 6)

	$a(365)$	$a(388)$	$a(480)$	$cp(365)$	$cp(388)$	$cp(480)$	$F(ex365/em460)$	$F(ex388/em490)$
$a(388)$	1.00							
$a(480)$	0.97	0.97						
$cp(365)$	0.92	0.93	0.77*					
$cp(388)$	0.91	0.91	0.76*	0.99				
$cp(480)$	0.91	0.91	0.74*	0.99	0.99			
$F(ex365/em460)$							0.88*	
$F(ex388/em490)$								1.00
$F(ex480/em543)$								
	0.95	0.94	0.92	0.91	0.89*	0.86*	0.99	0.98

All correlations are significant at  $P < 0.001$  except:

\* $P < 0.005$ .

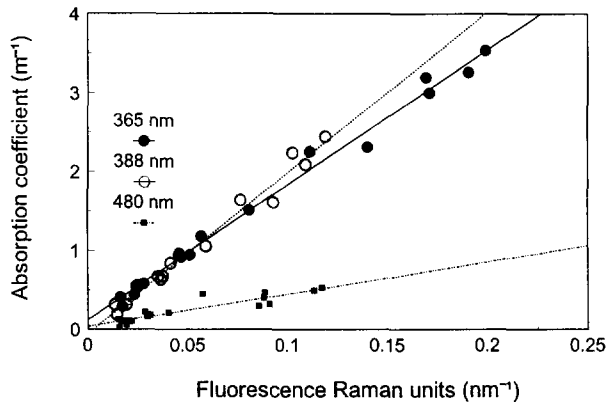


Fig. 6.  $F_{CDOM}$  at 460, 490 and 543 nm vs  $a_{CDOM}$  at 365, 388, and 480 nm, respectively.

$$a_{CDOM}(388) = 20.36 (\pm 0.38) F_{CDOM}(ex388/em490) - 0.05 (\pm 0.03) \quad (3)$$

$$a_{CDOM}(480) = 4.09 (\pm 0.04) F_{CDOM}(ex480/em543) - 0.04 (\pm 0.05). \quad (4)$$

Equations (2) and (3) in the UV range are similar, but they differ from equation (4) in the visible range. After appropriate transformations that account for differences in normalization and standardization (see Appendix), equation (2) is similar to that found by Hoge *et al.* (1993) for measurements at 355 nm.

#### 4. DISCUSSION

##### 4.1. Oceanographic processes in the St. Lawrence system

The observed variables reflect the main regional and local characteristics of water circulation. Variability in phytoplankton biomass (chl + phaeo) can be ascribed to the

influence of specific hydrographic features which are known for the Upper Estuary (Therriault *et al.*, 1990), the Lower Estuary (Therriault and Levasseur, 1986; Therriault *et al.*, 1990), and the Gulf of St. Lawrence (De Lafontaine *et al.*, 1991). For example, Stas 10–14, with high salinity (28 psu), low temperature (*ca* 5°C), and low chl + phaeo concentrations (*ca* 1 mg m<sup>-3</sup>), probably reflect the upwelling of subsurface waters (see Therriault and Lacroix, 1976). The high salinity (*ca* 29 psu), low temperature (<4°C), and low chl + phaeo values at Sta. 19 are probably indicative of recently upwelled waters in the divergence zone which often develop on both sides of the Manicouagan and Aux-Outardes plume (El-Sabh, 1979). In the Gulf, except at Sta. 32, which is under the influence of the outflow from the Gaspé Current, water mass characteristics of Stas 31–36 are typical of Case 1 waters, which reflect their oceanic origin. These findings are consistent with earlier studies in the Estuary and the Gulf of St. Lawrence, thus confirming the classification by Babin *et al.* (1993) of waters in the Upper and Lower Estuary as Case 2 and in the Gulf (Stas >24) as typical Case 1 mesotrophic waters.

#### 4.2. Fluorescence tracer of surface circulation

The strong correlations between both  $a_{\text{CDOM}}$  and  $F_{\text{CDOM}}$  and salinity and between  $a_{\text{CDOM}}$  and  $F_{\text{CDOM}}$  observed in this study suggest that these absorption and fluorescence variables can be considered as conservative properties of water masses and, therefore, may be used to track the surface circulation (characterized by salinity) in the Estuary and the Gulf of St. Lawrence. For the Lower Estuary and the Gulf, where phytoplankton abundance did not influence the relationship between salinity and both  $a_{\text{CDOM}}$  and  $F_{\text{CDOM}}$ , *in situ* production of CDOM can even be excluded. Strong linear relationships between  $F_{\text{CDOM}}$  and salinity have also been found in the coastal and estuarine waters of the North Sea and Wadden Sea (Kalle, 1949; Zimmerman and Rommets, 1974) and the nearshore area off the southeastern coast of the United States (Dorsch and Bidlemann, 1982). The important implication of this result is that, because  $F_{\text{CDOM}}$  can be remotely sensed with a fluorescence lidar on board an airplane or a ship with a laser excitation wavelength in the UV, this variable can be used as a surrogate measure of the salinity field. In this way, major hydrographic features could be observed by remote sensing.

In case of simultaneous detection of chl *a* fluorescence and  $F_{\text{CDOM}}$ , a laser wavelength in the visible range, close to the absorption maximum of chl *a* (e.g. 435–440 nm), would be needed. However, the signal intensity of  $F_{\text{CDOM}}$  is rather weak when excited at 388 and 480 nm, compared to that at 365 nm. Therefore, using 388 and 480 nm as excitation wavelengths should lead to lower precision in salinity estimates. Weak signals can affect the precision of salinity estimates. In case of small errors in fluorescence measurements, high errors in salinity estimates will be produced. In addition, the transition from Case 2 to Case 1 waters in the St. Lawrence system, as expressed by a slope discontinuity in the relationship between salinity and  $F_{\text{CDOM}}$  excited at 365 and 388 nm, cannot be observed at 480 nm. Therefore, efficient detection of  $F_{\text{CDOM}}$  in this wavelength range with a lidar would be best achieved by using a dual excitation lidar system providing an excitation wavelength in the UV for water mass classification and another in the visible dedicated to estimation of chl *a* biomass.

The observed change in slopes, for 365 and 388 nm in the transition zone between the Lower Estuary and the Gulf, indicates that the composition of absorbing and/or fluorescing molecules changed. Wavelength-specific absorption and fluorescence properties of

CDOM indicate that the chemical composition of the dissolved organic matter (DOM) pool and, hence, the relative concentrations of absorbing and fluorescent matter, were likely not the same for waters in the Estuary and the Gulf. Similar changes in the slopes of the relationships between fluorescence and salinity, related to different water types (i.e. different DOM composition), have also been found in the German Bight and Tokyo Bay, Japan (Reuter *et al.*, 1993; Hayase *et al.*, 1987). Willey and Atkinson (1982) also reported changes in the slopes of linear relationships between  $F_{\text{CDOM}}$  and salinity, for low salinity levels in the mixing areas of estuaries in Georgia and North Carolina. These authors found that this behaviour was not related to temperature, pH, or storage effect, but suggested possible interferences with chl *a*, lignin sulphates, detergents and oil.

#### 4.3. Estimation of CDOM absorption via CDOM fluorescence

Another interesting implication of our results is the possibility of deriving absorption estimates of CDOM from remotely sensed CDOM fluorescence data in the visible range (480 nm). This could eventually lead to a better spatial knowledge of CDOM absorption properties, a key parameter in many primary production models, and thus improve these models by providing more accurate estimates of the vertical distributions of light quality and intensity. Hoge *et al.* (1993) already presented such a relationship in the UV (337 and 355 nm) for different water masses. As already mentioned in the Results, the relationship between  $a_{\text{CDOM}}$  and  $F_{\text{CDOM}}$  in the St. Lawrence Estuary and Gulf at 365 nm [equation (2)] is similar to that described by Hoge *et al.* (1993) at 355 nm.

Differences between equations (2), (3) and (4) (see also Fig. 6) are related to spectral variations in the cross-section of the Raman scattering signal (see Lee *et al.*, 1994) and in the quantum yield of CDOM fluorescence (see Hawes *et al.*, 1992). The decrease in absorption toward longer wavelengths would thus not be proportional to the quantum yields of CDOM fluorescence. These variations can be related to changes in the composition of optically active molecules or simply because the energy of the absorbed quanta is so low that fluorescence emission by the molecule is no longer possible. The decrease in absorption toward longer wavelength would thus not be proportional to fluorescence emission. It follows that the relationship between  $a_{\text{CDOM}}$  and  $F_{\text{CDOM}}$  in the visible can be different from that in the UV.

In order to compute absorption from fluorescence with high accuracy, equations (2)–(4) must be verified with ground truth measurements for the absorption coefficient wavelengths of interest, e.g. 365, 388, or 480 nm excitation with 460, 490, or 543 nm emission, respectively. Respecting the association between the absorption coefficient and excitation wavelengths is crucial for such relationships. Also, changes in the coupled fluorescence excitation and emission can cause differences. For example, using equations (2)–(4) the same absorption and excitation wavelengths (365 and 480 nm) but a different fluorescence emission (450 and 620 nm instead of 460 and 543 nm, respectively) lead to slight changes in slope values, as shown in equations (5) and (6):

$$a_{\text{CDOM}}(365) = 17.97 F_{\text{FDOM}}(\text{ex}365/\text{em}450) + 0.09 \quad (5)$$

$$a_{\text{CDOM}}(480) = 3.20 F_{\text{FDOM}}(\text{ex}480/\text{em}620) + 0.08. \quad (6)$$

Calculations in the Appendix indicate that it is important to use standard normalization and standardization procedures in order to derive relationships that are widely applicable. For example, fluorescence intensities normalized to either part of the Raman signal or the

Raman peak, as described in Hoge *et al.* (1993), can only be compared directly if the exact same instrument configuration (e.g. identical slit widths) is used. However, some spectrofluorometers only have a limited choice of excitation and emission slit widths, which can make their data impossible to compare to other data. However, normalization to the Raman scattering cross-section allows direct comparison of fluorescence values in Raman units, which is independent of instrument configuration (Determann *et al.*, 1994).

Also, standardization to absolute values of the fluorescence signal, as in Hoge *et al.* (1993), using a quinine sulphate dihydrate (QS) solution for internal standard, is limited to the UV range. QS absorption decreases rapidly from the maximum at 350 nm to almost zero at 390 nm (Velapoldi and Mielenz, 1980). Thus, it is not possible to extend the use of this standard solution to 388 or 480 nm, so that we could not derive a relationship between  $a_{\text{CDOM}}$  and  $F_{\text{CDOM}}$  in the visible comparable to that in the UV. We therefore had to rely on Raman units to compare  $F_{\text{CDOM}}$  values for the relationship at 388 and 480 nm.

## 5. CONCLUSIONS

Measurements of  $F_{\text{CDOM}}$  and  $a_{\text{CDOM}}$  in the UV (365 and 388 nm) and visible (480 nm) ranges can be used as tracers for water mass identification and as a surrogate measure of the salinity field in the St. Lawrence system. At 365 and 388 nm, distinction between Case 2 and Case 1 waters is possible. At 480 nm, there was no difference in the relationships between  $a_{\text{CDOM}}$ ,  $F_{\text{CDOM}}$  and salinity in the transition zone between Case 2 and Case 1 waters. The estimated relationship between  $F_{\text{CDOM}}$  and  $a_{\text{CDOM}}$  at 365 nm excitation was consistent with previously published relationships for excitation at 337 and 355 nm (Hoge *et al.*, 1993). A similar relationship was also found for excitation at 388 nm. The estimation of  $a_{\text{CDOM}}$  and  $F_{\text{CDOM}}$  was found to be easier to compare among studies when using a simple normalization of  $F_{\text{CDOM}}$  values to the water Raman cross-section. Results reported here and those previously reported by Hoge *et al.* (1993) show the possibility of estimating  $a_{\text{CDOM}}$  from airborne lidar. Monitoring  $a_{\text{CDOM}}$  using the lidar technique could be highly useful for interpretation of the radiance signal at 412 nm, which will be detected by future ocean colour sensors. Such combined lidar-satellite operations would allow regional algorithms to be developed for detection of chlorophyll and other light absorbing substances in Case 2 waters. Detection and quantification of these substances from remote sensing are necessary for large-scale estimation of primary production. While chlorophyll concentration represents one of the main inputs in primary production models, it also determines with CDOM the vertical propagation of photosynthetically available radiation. Results reported here on the relationship between  $a_{\text{CDOM}}$  and  $F_{\text{CDOM}}$  in the visible spectral range demonstrate the feasibility of using lidar technology for modelling primary production of Case 2 waters.

*Acknowledgements*—This study was funded by grants from the Federal Minister of Research and Technology, Bonn (Germany), the Natural Sciences and Engineering Council of Canada, and the Department of Fisheries and Oceans (Canada). The authors thank L. Legendre and one anonymous reviewer for comments and suggestions, and technicians and students at the Maurice Lamontagne Institute for assistance with sampling. We are also grateful to the crew of the R.V. *Petrel V* for their support.

## REFERENCES

- André J. M. and A. Morel (1991) Atmospheric corrections and interpretation of marine radiances in CZCS imagery, revisited. *Oceanologica Acta*, **14**, 3–22.
- Austin R. W. (1977) Precision considerations in the measurement of volume attenuation coefficient. In: *Light in the Sea*, J. Tyler, editor, Drowden, Hutchinson and Ross, Stroudsburg, U.S.A., pp. 121–124.

- Austin R. W. and T. J. Petzold (1977) Considerations in the design and evaluation of oceanographic transmissometers. In: *Light in the Sea*, J. Tyler, editor, Drowden, Hutchinson and Ross, Stroudsburg, U.S.A., pp. 104–120.
- Babin M., J.-C. Therriault, L. Legendre and A. Condal (1993) Variations in the specific absorption coefficient for natural phytoplankton assemblages: impact on estimates of primary production. *Limnology and Oceanography*, **38**, 154–177.
- Baker K. S. and R. C. Smith (1982) Bio-optical classification and model of natural waters. 2. *Limnology and Oceanography*, **27**, 500–509.
- Benoît J., M. I. El-Sabh and C. L. Tang (1985) Structure and seasonal characteristics of the Gaspé current. *Journal of Geophysical Research*, **90**, 3225–3236.
- Bricaud A., A. Morel and L. Prieur (1981) Absorption by dissolved organic matter of the sea (yellow substance) in the UV and visible domains. *Limnology and Oceanography*, **26**, 43–53.
- Bristow M., D. H. Bundy, C. M. Edmonds, P. E. Ponto, B. E. Frey and L. F. Small (1985) Airborne laser fluorosensor survey of the Columbia and Snake rivers: simultaneous measurements of chlorophyll, dissolved organics and optical attenuation. *International Journal of Remote Sensing*, **6**, 1707–1734.
- Brunel P. (1970) Les grandes divisions du Saint-Laurent: 3<sup>ème</sup> commentaire. *Revue Géographie Montréal*, **24**, 291–294.
- Carder K. L., S. K. Hawes, K. A. Baker, R. C. Smith, R. G. Steward, and B. G. Mitchell (1991) Reflectance model for quantifying chlorophyll *a* in the presence of productivity degradation products. *Journal of Geophysical Research*, **96**, 599–520, 611.
- Carder K. L., R. G. Steward, J. H. Paul and G. A. Vargo (1986) Relationships between chlorophyll and ocean color constituents as they affect remote-sensing reflectance models. *Limnology and Oceanography*, **31**, 403–413.
- Chen R. F. and J. L. Bada (1992) The fluorescence of dissolved organic matter in seawater. *Marine Chemistry*, **37**, 191–221.
- Childs A. F. (1989) Removing the instrument function from fluorescence spectra. In: *Proceedings of Fluorescence Detection III*, Vol. 1054, SPIE, Los Angeles, pp. 8–19.
- De Lafontaine Y., S. Demers and J. Runge (1991) Pelagic food web interactions and productivity in the Gulf of St. Lawrence: a perspective. In: *The Gulf of St. Lawrence: Small Ocean or Big Estuary?* J.-C. Therriault, editor, Can. Spec. Publ. Fish. Aquat. Sci. 113, Fisheries and Oceans Canada, Mont-Joli, QC, Canada, pp. 99–124.
- Determann S., R. Reuter, P. Wagner and R. Willkomm (1994) Fluorescent matter in the eastern Atlantic Ocean Part 1: method of measurement and near-surface distribution. *Deep-Sea Research*, **41**, 659–675.
- Diebel D. (1987) *Tiefenaufgelöste Laserfernerkundung geschichteter Strukturen im Meer unter Verwendung von Gelbstoff als Tracersubstanz*, Ph.D. thesis, University of Oldenburg, Germany.
- Diehl P. and H. Haardt (1980) Measurement of the spectral attenuation to support biological research in a “plankton tube” experiment. *Oceanologica Acta*, **3**, 89–96.
- Doerffer R. (1979) Untersuchungen über die Verteilung oberflächennaher Substanzen im Elbe-Ästuar mit Hilfe von Fernmeßverfahren. *Archiv für Hydrobiologie Supplement*, **43**, 119–224.
- Dorsch J. E. and T. F. Bidleman (1982) Natural organics as fluorescent tracers of river-sea mixing. *Estuary, Coastal and Shelf Science*, **15**, 701–707.
- Duursma E. K. (1974) The fluorescence of dissolved organic matter in the sea. In: *Optical Aspects of Oceanography*, N. G. Jerlov and E. Steemann Nielsen, editors, Academic Press, London, pp. 237–256.
- El-Sabh M. I. (1976) Surface circulation pattern in the Gulf of St. Lawrence. *Journal of Fisheries Research Board Canada*, **33**, 124–138.
- El-Sabh M. I. (1979) The Lower St. Lawrence Estuary as a physical oceanographic system. *Le Naturaliste Canadien*, **106**, 55–73.
- El-Sabh M. I., E. Bourget, M. J. Bowers and J. C. Dionne (1979) Oceanography of the St. Lawrence Estuary. *Le Naturaliste Canadien*, **106**, 276.
- Forrester W. D. (1974) Internal tides in the St. Lawrence Estuary. *Marine Research*, **32**, 55–66.
- Glantz S. A. (1992) *Primer of Bio-statistics*, McGraw-Hill, New York.
- Gordon H. R. and A. Morel (1983) *Remote Assessment of Ocean Color for Interpretation of Satellite Visible Imagery; A Review*, Springer-Verlag, Heidelberg, 114 pp.
- Haardt H., P. Diehl and B. Knoppers (1979) *Messungen des spektralen Attenuationskoeffizienten an Latexsuspensionen, Phytoplanktonkulturen und natürlichen Wasserproben aus der Ostsee*, Reports Sonderforschungsbereich 95, No. 52, Kiel University, Kiel, FRG, 62 pp.

- Hawes S. K., K. L. Carder and G. R. Harvey (1992) Quantum fluorescence efficiencies of fulvic and humic acids: effects on ocean color and fluorometric detection. *SPIE*, **1750**, 212–223.
- Hayase K., M. Yamamoto, I. Nakazawa and H. Tsubota (1987) Behavior of natural fluorescence in Sagami Bay and Tokyo Bay, Japan—vertical and lateral distributions. *Marine Chemistry*, **20**, 265–276.
- Hoge F. E. and R. N. Swift (1982) Delineation of estuarine fronts in the German Bight using airborne laser-induced water Raman backscatter and fluorescence of the water column constituents. *International Journal of Remote Sensing*, **3**, 475–495.
- Hoge F. E., A. Vodacek and N. V. Blough (1993) Inherent optical properties of the ocean: retrieval of the absorption coefficient of chromophoric dissolved organic matter from fluorescence measurements. *Limnology Oceanography*, **38**, 1394–1402.
- Holm-Hansen O., C. J. Lorenzen, R. W. Holmes and J. D. H. Strickland (1965) Fluorometric determination of chlorophyll. *J. Cons. Perm. Int. Explor. Mer.*, **30**, 3–15.
- Kalle K. (1938) Zum Problem der Meerwasserfarbe. *Ann. Hydrol. Mar. Mitt.*, **66**, 1–13.
- Kalle K. (1949) Fluoreszenz und Gelbstoff im baltischen und finnischen Meerbusen. *Deutsche Hydrographische Zeitschrift*, **2**, 117–124.
- Kalle K. (1963) Über das Verhalten und die Herkunft der in den Gewässern und in der Atmosphäre vorhandenen himmelblauen Fluoreszenz. *Deutsche Hydrographische Zeitschrift*, **16**, 153–166.
- Koutitonsky V. G. and G. L. Budgen (1991) The physical oceanography of the Gulf of St. Lawrence: a review with emphasis on the synoptic variability of the motion. In: *The Gulf of St. Lawrence: Small Ocean or Big Estuary?*, Vol. 113, J.-C. Theriault, editor, Fisheries and Oceans Canada, Mont-Joli, QC, Canada, pp. 57–90.
- Lee Z., K. L. Carder, S. K. Hawes, R. G. Steward, T. G. Peacock and C. O. Davis (1994) Model for the interpretation of hyperspectral remote-sensing reflectance. *Applied Optics*, **33**, 5721–5732.
- Lundgren B. (1976) *Spectral Transmittance Measurements in the Baltic Sea*, Report No. 30, Københavns Universitet, Institut for Fysisk Oceanografi, Copenhagen, 38 pp.
- Maul G. A. and H. R. Gordon (1975) On the use of the earth resources technology satellite (LANDSAT-1) in optical oceanography. *Remote Sensing of Environment*, **4**, 95–128.
- Morel A. (1988) Optical modeling of the upper ocean in relation to its biogenous matter content (case 1 waters). *Journal of Geophysical Research*, **93**, 749–710, 768.
- Morel A. and L. Prieur (1976) Analyse spectrale de l'absorption par les substances dissoutes (substances jaunes). In: *Résultats de la Campagne CINECA V*, Vol. 1.1.11, CNEXO, France, 39 pp.
- Morel A. and L. Prieur (1977) Analysis of variations in ocean color. *Limnology and Oceanography*, **22**, 709–722.
- Neu H. J. A. (1970) A study on mixing and circulation in the St. Lawrence estuary up to 1964. *Atlant. Oceanogr. Lab. Bed. Inst. Rep. Ser.*, **1970–1979**, 31.
- Platt T. and S. Sathyendranath (1988) Oceanic primary production: estimation by remote sensing at local and regional scales. *Science*, **241**, 1613–1620.
- Reuter R., D. Diebel and T. Hengstermann (1993) Oceanographic laser remote sensing: measurement of hydrographic fronts in the German Bight and the Northern Adriatic Sea. *International Journal of Remote Sensing*, **14**, 823–848.
- Reuter R., D. Diebel-Langohr, R. Doerffer, F. Dörre, H. Haardt and T. Hengstermann (1986) Optical properties of gelbstoff. In: *The Influence of Yellow Substances on Remote Sensing of Seawater Constituents from Space*, Vol. 2, GKSS Geesthacht Research Center, Geesthacht, Germany, p. 58.
- Spitz A. and V. Ittekkott (1986) Gelbstoff: an uncharacterized fraction of dissolved organic carbon. In: *The Influence of Yellow Substances on Remote Sensing of Sea-water Constituents from Space*, Vol. 2, GKSS Geesthacht Research Center, Geesthacht, Germany, p. 31.
- Tang C. T. (1980) Mixing and circulation in the northwestern Gulf of St. Lawrence: a study of a buoyancy-driven current system. *Journal of Geophysical Research*, **85**, 2787–2796.
- Theriault J.-C. and G. Lacroix (1976) Nutrients, chlorophyll and internal tides in the St. Lawrence Estuary. *Journal of Fisheries Research Board Canada*, **33**, 2747–2757.
- Theriault J.-C. and M. Levasseur (1985) Control of phytoplankton production in the lower St. Lawrence Estuary: light and freshwater run-off. *Le Naturaliste Canadien*, **112**, 77–96.
- Theriault J.-C. and M. Levasseur (1986) Freshwater runoff control of the spatio-temporal distribution of phytoplankton in the Lower St. Lawrence Estuary (Canada). In: *Proceedings of the NATO Freshwater/Sea Workshop, Bodo, Norway*, Vol. G7, S. Skreslet, editor, Springer Verlag, New York, pp. 251–260.
- Theriault J.-C., L. Legendre and S. Demers (1990) Oceanography and ecology of phytoplankton in the St. Lawrence Estuary. *Coastal Estuary Studies*, **39**, 269–295.

- Therriault J.-C., J. Painchaud and M. Levasseur (1985) Factors controlling the occurrence of *Protogonyaulax tamarensis* and shellfish toxicity in the St. Lawrence Estuary: freshwater runoff and the stability of the water column. In: *Toxic Dinoflagellates*, A. Anderson, W. White and Baden, editors, Elsevier, Amsterdam, pp. 141–146.
- Traganza E. D. (1969) Fluorescence excitation and emission spectra of dissolved organic matter in sea water. *Bulletin of Marine Science*, **19**, 897–904.
- Velapoldi R. A. and K. D. Mielenz (1980) *A Fluorescence Standard Reference Material: Quinine Sulfate Dihydrate: NBS Special Publication SP 260-64*, National Bureau of Standards, Washington, DC, 139 pp.
- Wiley J. D. (1984) The effect of seawater magnesium on natural fluorescence during estuarine mixing, and implications for tracer applications. *Marine Chemistry*, **15**, 19–45.
- Wiley J. D. and L. P. Atkinson (1982) Natural fluorescence as a tracer for distinguishing between Piedmont and coastal plain river water in the nearshore waters of Georgia and North Carolina. *Estuarine, Coastal and Shelf Science*, **14**, 49–59.
- Yentsch C. S. and D. W. Menzel (1963) A method for the determination of phytoplankton chlorophyll and phaeophytin by fluorescence. *Deep-Sea Research*, **10**, 221–231.
- Zimmerman J. T. F. and J. W. Rommets (1974) Natural fluorescence as a tracer in the Dutch Wadden Sea and adjacent North Sea. *Netherlands Journal of Sea Research*, **8**, 117–125.

## APPENDIX

Hoge *et al.* (1993) investigated the relationship between absorption and fluorescence in the UV, at 337 and 355 nm for different water masses. They concluded that  $a_{\text{CDOM}}$  at 337 and 355 nm can be computed directly from  $F_{\text{CDOM}}$  at 430 and 450 nm emission wavelengths, respectively, using the following equations:

$$a_{\text{CDOM}}(337) = 0.183 F_{\text{CDOM}}(\text{ex}337/\text{em}430) + 0.158 \quad (\text{A1})$$

$$a_{\text{CDOM}}(355) = 0.207 F_{\text{CDOM}}(\text{ex}355/\text{em}450) + 0.112. \quad (\text{A2})$$

The 100 factor difference for the slopes of equations (A1) and (A2) as compared to equations (2)–(4) is related to the use of different normalization and standardization procedures. Hoge *et al.* (1993) normalized an 11 nm fluorescence band to an 11 nm band of the Raman signal. We used 1 nm bandwidth for the fluorescence emission, normalized to the integral of the Raman signal. Using an 11 nm band in our calculations led to a slope for the relationship between  $a_{\text{CDOM}}(365)$  and  $F_{\text{CDOM}}(\text{ex}365/\text{em}450)$  that agreed within a factor of 4 with the one found by Hoge *et al.* (1993) at 355 nm [equation (8)]:

$$a_{\text{CDOM}}(365) = 0.837 (\pm 0.03) F_{\text{CDOM}}(\text{ex}365/\text{em}460) + 0.09 (\pm 0.07). \quad (\text{A3})$$

Hoge *et al.* (1993) also standardized their fluorescence spectra with a Raman normalized solution of  $0.01 \text{ mg l}^{-1}$  quinine sulphate (QS) in 1 N  $\text{H}_2\text{SO}_4$  (0.01 ppm), which is one further dilution of the NBS standard (1980). They defined standardized fluorescence units (N.Fl.U.) as:

$$[(F_{\text{sample}}:R_{\text{sample}})/(F_{\text{QS}}:R_{\text{QS}}) \times 10 = F(\lambda) \text{ (N.Fl.U.)}] \quad (\text{A4})$$

where  $\lambda$  is the excitation wavelength, and  $F$  and  $R$  are the fluorescence and water Raman signal in the seawater or quinine sulphate sample, respectively.

Standardization of equation (A3), using equation (A4), leads to the following relationship between  $a_{\text{CDOM}}$  and  $F_{\text{CDOM}}$  at 365 nm, for our study:

$$a_{\text{CDOM}}(365) = 0.353 (\pm 0.012) F_{\text{CDOM}}(\text{ex}365/\text{em}460) + 0.17 (\pm 0.067). \quad (\text{A5})$$

The slope value of 0.353 is similar to the values reported by Hoge *et al.* (1993) for 337 nm [equation (A1)] and 355 nm [equation (A2)].

However, since we were using different slit widths for the excitation and emission paths (10 nm vs 4 nm), the initial Raman normalization to an 11 nm band instead of using the Raman integral must be corrected. Measurements of MILLIPORE water or the 0.01 ppm quinine sulphate solution, using exactly the same instrument configuration as for measuring the fluorescent spectra, allows, after a spectral correction, the slit width correction factor to be determined. This leads, from equation (A5), to the following relationship between  $a_{\text{CDOM}}$  and  $F_{\text{CDOM}}$  in the St. Lawrence:

$$a_{\text{CDOM}}(365) = 0.262 (\pm 0.009) F_{\text{CDOM}}(\text{ex}365/\text{em}460) + 0.10 (\pm 0.070) \quad (\text{A6})$$

which is similar to equation (A2) (355 nm, in the Delaware Bight) or Hoge *et al.* (1993).